

Highly uniform step and terrace structures on SiC(0001) surfaces

J. Sun
J. B. Hannon
R. M. Tromp
K. Pohl

Highly uniform step and termination structures on 4H- and 6H-SiC(0001) surfaces have been prepared via moderate annealing in disilane. Atomic force microscopy and dark-field low-energy electron microscopy imaging indicate single-phase terminations separated solely by half-unit-cell-height steps, driven by stacking fault energy. The atomic structure of 4H-SiC(0001)- $\sqrt{3} \times \sqrt{3}R30^\circ$ -Si has been determined quantitatively by nanospot low-energy electron diffraction. The topmost stacking fault at the 4H surface has been found to be between the second and third bilayers.

Introduction

Silicon carbide has been an important platform for epitaxial thin-film growth [1] and is currently considered a promising candidate for the epitaxial growth of graphene [2–4]. Since the performance of thin-film devices based on SiC substrates critically depends on the film quality, the SiC surface preparation and control are crucial due to its strong impact on epitaxial growth. Therefore, it is of fundamental significance to study the SiC surface structure that is mainly driven by the surface stacking fault energy. In this paper, we present a preparation method for highly uniform step and surface terminations on 4H- and 6H-SiC(0001) and the quantitative determination of the 4H-SiC(0001)- $\sqrt{3} \times \sqrt{3}R30^\circ$ -Si (4H- $\sqrt{3}$, for short) surface structure.

4H- and 6H-SiC are among the most stable and widely studied SiC polytypes. As their name indicates, 4H and 6H have four and six bilayers in their primitive unit cell, respectively, as shown in **Figure 1**. Consequently, the 4H and 6H surfaces have four and six possible terminations, respectively. The essential difference between 4H and 6H structures is the difference in the stacking position. It is safe to say that the surface termination is governed by the stacking fault location. We have employed annealing at a moderate temperature of 1,373 K in disilane to avoid some of the complications of high-temperature H₂ etching. Indeed, dark-field low-energy electron microscopy (LEEM) imaging

and atomic force microscopy (AFM) show only a single termination on the 4H- and 6H-SiC(0001) surfaces with uniform step heights of half-unit-cell length.

The challenge of determining the surface termination essentially lies in determining the stacking fault positions, which are indicated by broken lines in **Figure 1**. Despite a discernible total energy difference between different bulk stacking faults, identifying the stacking fault positions at surfaces is extremely difficult since the energy difference between different terminations is quite subtle. Thus, reliable experiential surface techniques to determine the buried stacking fault positions are urgently needed.

Most surface analytical tools such as low-energy electron diffraction (LEED), x-ray photoelectron spectroscopy, surface x-ray diffraction (XRD), and Raman spectroscopy are based on spatially averaged probing of micron-wide regions. Local structural probes such as scanning tunneling microscopy and AFM are based on surface scanning and are thus only imaging the topmost layer. In contrast, LEEM is an *in situ* real-time direct imaging technique capable of probing nanometer-wide surface regions [5–8]. As a novel quantitative analysis technique based on LEEM diffraction, we developed nanospot LEED (nLEED) to determine the surface atomic structure of 4H- $\sqrt{3}$. As an improvement over previous attempts of microdiffraction in LEEM (μ LEED) [9, 10], where a region of about 2 μ m is illuminated, we enhanced the resolution by an order of magnitude by restricting the illumination area to a single domain of about 200 nm. Compared with our recently developed LEEM intensity/voltage (I/V) technique, which

Digital Object Identifier: 10.1147/JRD.2011.2156230

© Copyright 2011 by International Business Machines Corporation. Copying in printed form for private use is permitted without payment of royalty provided that (1) each reproduction is done without alteration and (2) the Journal reference and IBM copyright notice are included on the first page. The title and abstract, but no other portions, of this paper may be copied by any means or distributed royalty free without further permission by computer-based and other information-service systems. Permission to republish any other portion of this paper must be obtained from the Editor.

0018-8646/11/\$5.00 © 2011 IBM

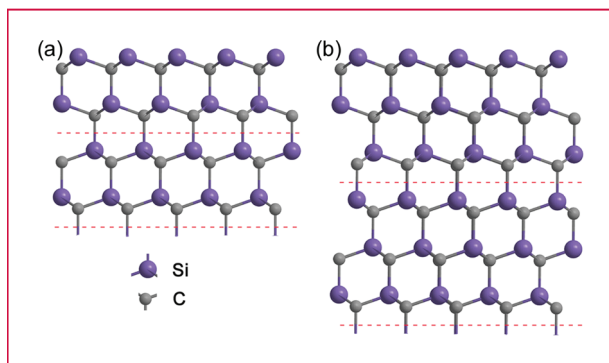


Figure 1

Silicon carbide. Side view of (a) 4H-SiC(0001) and (b) 6H-SiC(0001) repeated stacking bilayer units as projected onto the $(11\bar{2}0)$ plane. Large (purple) and small (gray) circles represent Si and C atoms, respectively. Stacking faults are indicated by broken lines. 4H and 6H have four and six possible terminations, respectively.

uses only the (00) beam at a spatial resolution of about 8.5 nm [11, 12], the novel nLEED technique provides a larger data set containing multiple beams at a cost of a slightly lower resolution. Compared with conventional LEED intensity analysis, this technique eliminates uncertainties in the domain size ratio and thus increases the technical reliability. Therefore, this paper is expected to provide more accurate and definite surface structure information.

Experiments

In the process of preparing SiC substrates, the scratches and damages on SiC after grinding and mechanical polishing are usually removed with chemical–mechanical polishing, H_2 etching, or reactive ion etching. H_2 etching at a high temperature (1,673–1,973 K) [1] is most effective and widely adopted, but it tends to result in narrow and nonuniform flat domains [13] or step bunching [14]. We use an alternative approach of disilane etching at around 1,373 K. The successful attainment of uniform step and terrace structures is attributed to the multiple roles of disilane, i.e., etching to eliminate the mechanical damages, cleaning to remove surface contaminants, and supplying Si to avoid any surface graphitization.

4H- and 6H- $\sqrt{3}$ surfaces are obtained by annealing at an elevated temperature of about 1,373 K at a background pressure of disilane at about 10^{-6} torr [15]. This Si-reconstructed surface is stabilized by reduction of the dangling bonds on the 1×1 structure, similar to the metal-adsorbed Si(111) surface. We chose the $\sqrt{3}$ structure since it had been better characterized than other superstructures such as 1×1 , 3×3 , or $6\sqrt{3} \times 6\sqrt{3}$. Most structural studies of the $\sqrt{3} \times \sqrt{3}$ SiC structure have been

performed on the 6H- $\sqrt{3}$ surface [16–23], whereas only one experimental [24] and some theoretical [15, 21] studies have been reported on the 4H- $\sqrt{3}$ surface. *In situ* LEEM electron imaging and diffraction have been performed to observe the surface phases and to collect reflectivity spectra. All the LEEM experiments were performed in an ultrahigh-vacuum chamber with a base pressure of $\sim 1.0 \times 10^{-10}$ torr. The surfaces were investigated in the dark-field imaging mode, i.e., by deflecting the incident electron beam, so that a nonspecular beam is directed through the aperture to image the surface. AFM has been used to confirm the step heights of all samples.

LEEM can be instantly switched to the conventional LEED working mode by removing the aperture in the back focal plane and tuning the relevant electronic lens. In the IBM LEEM-II system used, the illumination selector can be set to restrict the incident beam onto a very small area of the surface [6]. An illumination region of 200 nm in diameter is routinely achievable.

Dynamical electron diffraction intensity analysis

I/V curves are calculated for trial structures and compared with the experiment. The parameters of the trial structure are varied to give the best agreement with the measurement. The standard package symmetrized automated tensor LEED [25] has been used. Up to nine phase shifts [26] ($L = 8$) were used for the atomic t -matrix calculation. Four symmetry-inequivalent beams, i.e., (0,0), (1,0), (0,1), and (1/3,1/3), at normal incidence were compared. An R_P reliability factor [27] was employed to measure the agreement level between the experimental and theoretical data. It is assumed that the residual value of R_P at the minimum value $R_{P \min}$ is $\Delta R_P = R_{P \min} \times \sqrt{8|V_{\text{im}}|/\Delta E}$, where V_{im} is the imaginary part of the inner potential, and ΔE is the total energy range analyzed. From this residual and the curvature of R_P near the minimum, we can estimate the uncertainty in the optimized parameters.

The electron kinetic energy values in the LEEM experiments (10–150 eV) are usually lower than those in the conventional LEED experiments (50–500 eV). This low-energy range can complicate the quantitative analysis because, within about 50 eV of the vacuum level, the mean free path of electrons in solids is strongly energy dependent [28]. Consequently, in calculations of the electron reflectivity, the inelastic damping potential (i.e., the imaginary part of inner potential V_{im}) cannot be assumed to be constant as in the conventional LEED I/V technique. In our calculation, we use the optical potential in the form of $V_{\text{im}}(E) = V_{\text{damp}}E^{1/3}$, as proposed for low-index Ni [29] and Cu surfaces [30, 31]. We optimized the constant prefactor V_{damp} as an independent nonstructural parameter, and the best fit value is 0.66. We included an overall constant shift V_0 for the real part of the inner potential as another nonstructural parameter. The Debye temperature of the bulk

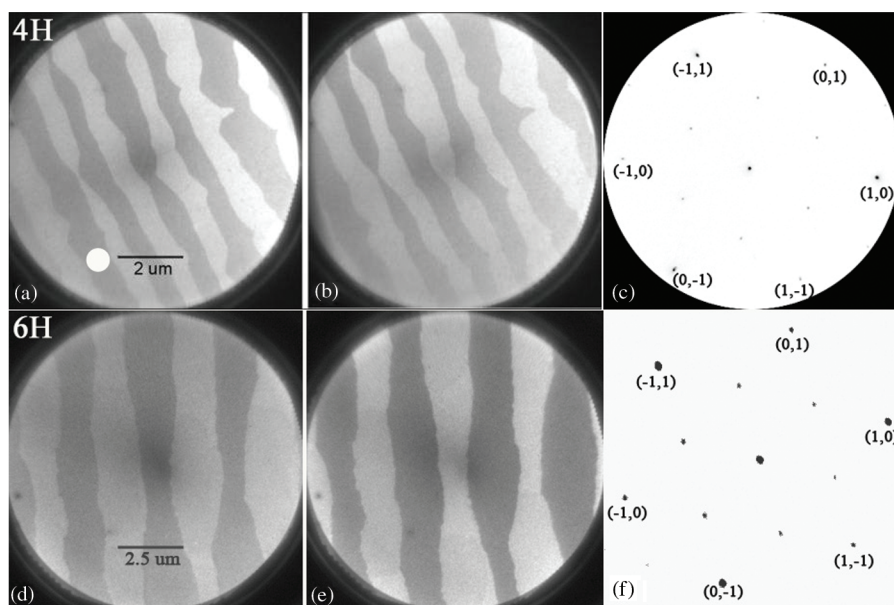


Figure 2

Imaging. Dark-field images at 14.7 eV with (a) beam (1,0) and (b) beam (0,1) for $4H-\sqrt{3}$. (d) and (e) Corresponding images at 14.6 eV for $6H-\sqrt{3}$. Contrast-inverted diffraction patterns (c) at 23 eV and (f) at 50 eV are from single $4H-\sqrt{3}$ and $6H-\sqrt{3}$ terraces, respectively. The first-order beams are labeled, which show threefold symmetry in intensity. The white spot in (a) indicates the illumination area in nLEED patterns.

is fixed at 1,300 K [32], whereas the atomic vibrational amplitude for the first layer is adjusted. LEEM diffraction images contain a contribution from inelastically scattered (and secondary) electrons. This contribution is directly measured by integrating the background intensity and has been deducted.

Results and discussion

Step and terrace structures

In LEEM dark-field imaging, we used the (1,0) and (0,1) beams to compare the reflectivity values of the terraces. **Figures 2(a)** and **2(b)** show images taken with these two beams for $4H-\sqrt{3}$, respectively, and **Figures 2(d)** and **2(e)** show the corresponding images for $6H-\sqrt{3}$. First, we see that every other domain has the same reflectivity, which indicates that the same termination appears across two steps. Second, the complete contrast reversal between **Figures 2(a)** and **2(b)** and between **Figures 2(d)** and **2(e)** suggests that neighboring terraces are indeed rotated by 60° with respect to each other. These observations lead to a conclusion that the step heights are of half-unit-cell length since the terminations in $4H$ and $6H$ separated by a half-unit-cell height are equivalent to each other by a rotation of 60° .

Our AFM measurements also verified our conclusion. As a result, there are only two possible terminations on the $4H-\sqrt{3}$ surface, and we denote S_1 and S_2 as terminations with the topmost stacking fault underneath the first and second bilayers, respectively. Similarly, we denote three possible terminations on the $6H-\sqrt{3}$ surface, i.e., S_1 , S_2 , and S_3 , as terminations with the topmost stacking fault underneath the first, second, and third bilayers, respectively.

In this paper, the single-domain width is about 600 nm for $4H-\sqrt{3}$, and we illuminated the entire uniform area, as shown by the white circular spot in the bottom left part of **Figure 2(a)**, to reduce the statistical error. The sharp diffraction pattern at 23 eV is shown in **Figure 2(c)**. It shows threefold rotational symmetry among the first-order beams, i.e., the (1,0), (-1,1), and (0,-1) beams have the same intensity, different from the same intensity among beams (0,1), (-1,0), and (1,-1). It suggests single-domain diffraction and rules out contributions from two neighboring domains, which would give a sixfold symmetric pattern. Diffraction spectra, i.e., LEED I/V curves, are measured by ramping the electron kinetic energy from 20 to 100 eV. A diffraction pattern at 50 eV from a single terrace of $6H-\sqrt{3}$ is shown in **Figure 2(f)**, and the threefold rotational symmetry also holds.

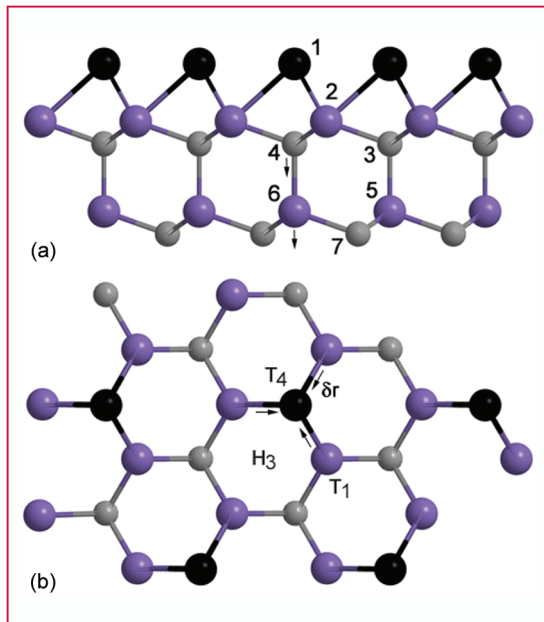


Figure 3

Structural models. (a) Side view of bulk-terminated $4H-\sqrt{3}$ with the T_4 -site overlayer registry. Large (purple/black) and small (gray) circles represent Si and C atoms, respectively. The numbers are layer labels. Arrows indicate downward rippling directions of sublattice atoms 4 and 6. (b) Top view of T_4 , T_1 , and H_3 sites of the $4H-\sqrt{3}$ surface; only one bulk bilayer is shown. δr is the radial displacement of the second-layer Si atoms relative to the T_4 -site adlayer Si atom.

4H- and 6H- $\sqrt{3}$ surface structures

A $4H-\sqrt{3}$ superstructure model has been previously proposed and tested both experimentally [24] and theoretically [21]. The consensus is that the $\sqrt{3}$ adlayer is a T_4 -site Si layer, i.e., the topmost Si atoms are above the second-layer C atoms. This model is shown in **Figure 3**. T_1 and H_3 sites are also indicated in Figure 3(b). For each of two possible bulk terminations, we first tested all three possible sites and have found that the T_4 model gives a much better fit than the T_1 or H_3 model. In the next step, we compared the T_4 site on two bulk terminations. After careful analysis, it is found that termination S_2 has much better agreement than termination S_1 with the experimental data. This is indicated by a smaller reliability factor for S_2 ($R_p = 0.19$) than that for S_1 ($R_p = 0.44$). To visualize the difference in the level of agreement, I/V curves are plotted for these two models against the experimental data, as shown in **Figure 4**. The black solid curves represent the experimental data; the red solid and dotted blue curves represent the best fit data for terminations S_2 and S_1 , respectively. It is obvious that termination S_2 shows much better agreement than S_1 termination. For example, the peak at around 45 eV in beam (1,0) does not appear at all for S_1 termination. The superstructure obtained based on termination S_2 , as described

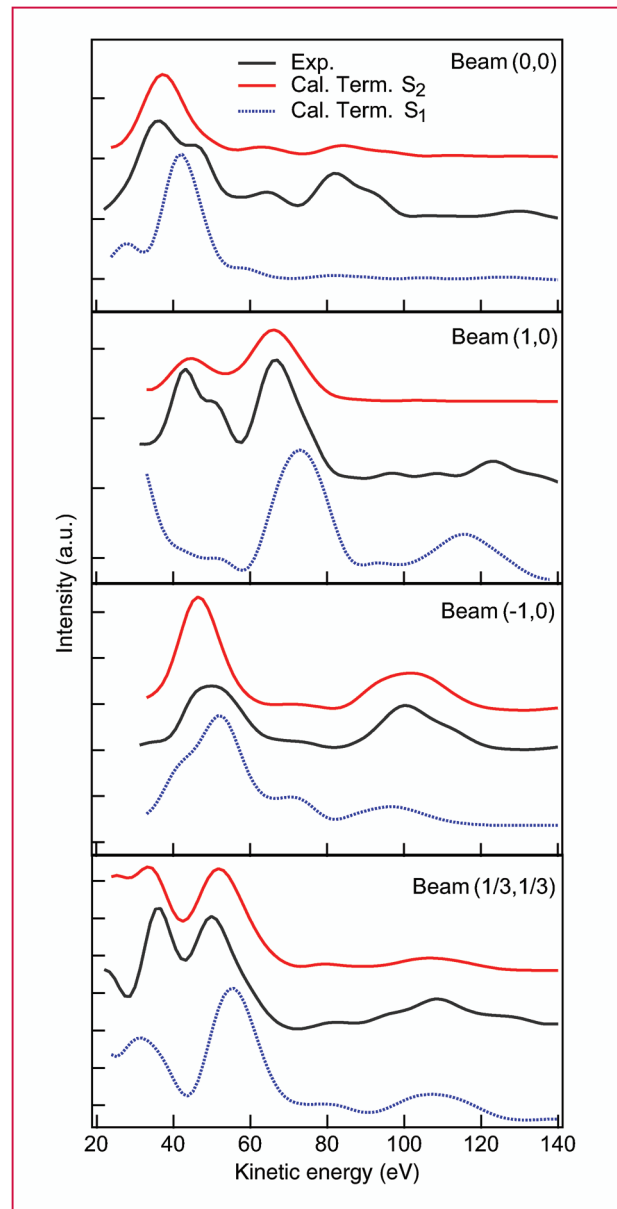


Figure 4

I/V spectra for $4H-\sqrt{3}$. (Black solid line) Experimental curves. (Red solid line) Best-fit curves for termination S_2 . (Dotted blue line) Best-fit curves for termination S_1 .

below, shows a structure similar to the previously reported one. In contrast, the optimized structure based on termination S_1 is a nearly bulk-terminated surface, which, in addition to a much larger R -factor, is not favorable because of a large number of exposed dangling bonds. Thus, we conclude that the stacking faults are situated between the second and third bilayers.

The optimized values for the interlayer spacings are denoted by d_i ($i = 1, \dots, 6$), i.e., the spacing between the i th

Table 1 Optimum parameter values compared with previous experimental and theoretical results. The interlayer spacing between the i th and $(i + 1)$ th layers is denoted by d_i . δr is the radial atomic displacement toward the threefold symmetry axis through the T_4 site. (DFT: density functional theory; LEED: low-energy electron diffraction; GXRD: grazing incidence x-ray diffraction, RHEED: reflection high-energy electron diffraction; PED: photoelectron diffraction.)

Methods [reference]	d_1	d_2	d_3	d_4	d_5	d_6	δr (Å)
LEEM (this work)	1.71	0.37	0.38	1.65	0.17	0.47	0.05
DFT [16]	1.75	0.57	0.22	1.72	0.10	0.56	0.06
LEED [24]	1.77	0.29	0.34	—	0.12	—	0.07
GXRD [18]	1.61	0.36	0.43	—	0.10	—	—
RHEED [22]	1.68	0.63	0.24	—	—	—	0.13
PED [23]	1.70	0.48	0.11	—	—	—	0.15

and $(i + 1)$ th layers. These layer numbers are also shown in Figure 3(a). In the bulk-terminated surface, layers 3 and 4 (as well as 5 and 6) are actually in the same layer, but buckling due to the $\sqrt{3}$ superstructure splits them into two sublayers. d_3 and d_5 denote the bucklings in the second and third layers, respectively. The T_4 -site-induced radial displacement of the atoms in the first layer is possible while retaining the threefold rotation symmetry. This displacement δr relative to the threefold symmetry axis through the T_4 site is schematically shown in Figure 3(b). The optimum values of the main structural parameters are as follows: first interlayer spacing $d_1 = 1.71$ Å, second-layer buckling $d_3 = 0.38$ Å, third-layer buckling $d_5 = 0.17$ Å, and $\delta r = 0.05$ Å. The best fit structural parameters are summarized in **Table 1**, together with reported results from previous work. The Debye temperature for the topmost layer is found to be 500 K, much lower than the value of $1,300 \pm 200$ K for the bulk, which is characteristic of a soft surface layer. The real part of the inner potential, or the muffin-tin zero, is found to be 11.0 ± 1.5 eV. We estimate the errors in terms of a deviation of minimum R_p factor, i.e., $\Delta R_p = 0.04$ with $V_{im} = -2.7$ eV at $E = 70$ eV, and $\Delta E = 448$ eV. This accumulated energy range could lead to an overestimation of the error bars, via ΔR_p , compared with more typical values of about 1,500 eV in conventional LEED analysis. Hence, the conservative errors in the interlayer spacing are about 0.06 Å for the nonbuckled layers and about 0.04 Å for the buckled layers. It is noticeable that an evident buckling in the third layer, i.e., d_5 , occurs reflecting a deep impact from the surface reconstruction. Compared with most previous studies, we have obtained relaxation information down to the sixth layer. Considering the advantages of the nLEED technique over conventional LEED, we believe that our model is a more precise representation of the real surface structure.

As mentioned earlier, the $6H\text{-}\sqrt{3}$ surface exhibits step heights of half-unit-cell length, and the surface termination

must be one of the three possible ones, i.e., S_1 , S_2 , or S_3 . We performed single-domain diffraction, extracted the I/V spectra, and found that the spectral shapes and structures are very similar to those for $4H\text{-}\sqrt{3}$. In our intensity analysis, termination S_1 could be ruled out, but it was difficult to distinguish terminations S_2 and S_3 . This is not surprising, considering that terminations S_2 and S_3 have the same topmost five layers, i.e., one $\sqrt{3}$ layer and two bilayers. However, according to the findings that cubic growth is preferred on $4H\text{-}\sqrt{3}$ [15], it is expected that termination S_3 is favored over S_2 . This indicates a trend that the stacking faults tend to be far away from the surface in order to minimize the surface stacking fault energy. This conclusion is also supported by concurrent first-principles calculations (private communication, V. B. Shenoy, Brown University).

Summary

LEEM and AFM investigations have shown uniform steps and terminations on $4H\text{-}$ and $6H\text{-SiC}(0001)$ surfaces, as prepared via moderate annealing in the ambient of disilane. By the novel quantitative nLEED technique, the surface structure of $4H\text{-}\sqrt{3}$ has been determined, and the stacking faults have been found to be between the second and third bilayers. The stacking fault position is suggested to be between the third and fourth bilayers for $6H\text{-SiC}(0001)$.

Acknowledgments

This work was supported in part by the Defense Advanced Research Projects Agency under Contract FA8650-08-C-7838 through the Carbon Electronics for Radio-Frequency Applications Program, by the Petroleum Research Fund under Grant 46323-AC5, and by the National Science Foundation under Grant DMR-1006863.

References

1. W. Choyke, H. Matsunami, and G. Pensl, *Silicon Carbide: Recent Major Advances*. New York: Springer-Verlag, 2004.
2. C. Berger, Z. Song, T. Li, X. Li, A. Ogbazghi, R. Feng, and W. de Heer, "Ultrathin epitaxial graphite: 2D electron gas properties and a route toward graphene-based nanoelectronics," *J. Phys. Chem. B*, vol. 108, no. 52, pp. 19 912–19 916, Dec. 2004.
3. A. K. Geim and K. S. Novoselov, "The rise of graphene," *Nat. Mater.*, vol. 6, no. 3, pp. 183–191, Mar. 2007.
4. R. M. Tromp and J. B. Hannon, "Thermodynamics and kinetics of graphene growth on SiC(0001)," *Phys. Rev. Lett.*, vol. 102, no. 10, p. 106104, Mar. 2009.
5. E. Bauer, "Low energy electron microscopy," *Rep. Prog. Phys.*, vol. 57, no. 9, pp. 895–938, Sep. 1994.
6. R. M. Tromp, "Low energy electron microscopy," *IBM J. Res. Dev.*, vol. 44, no. 4, pp. 503–516, 2000.
7. M. S. Altman, "Trends in low energy electron microscopy," *J. Phys. Condens. Matter.*, vol. 22, no. 8, p. 084017, Feb. 2010.
8. D. P. Woodruff, "The structure of surfaces: What do we know and what would we like to know?" *J. Phys. Condens. Matter.*, vol. 22, no. 8, p. 084016, Feb. 2010.
9. J. de la Figuera, J. Puerta, J. Cerda, F. E. Gabaly, and K. McCarty, "Determining the structure of Ru(0001) from low-energy electron diffraction of a single terrace," *Surf. Sci.*, vol. 600, no. 9, pp. L105–L109, May 2006.
10. K. R. Knox, S. Wang, A. Morgante, D. Cvetko, A. Locatelli, T. O. Montes, M. A. Niño, P. Kim, and J. R. M. Osgood, "Spectromicroscopy of single and multilayer graphene supported by a weakly interacting substrate," *Phys. Rev. B*, vol. 78, no. 20, p. 201408, Nov. 2008.
11. J. Sun, J. B. Hannon, G. L. Kellogg, and K. Pohl, "Local structural and compositional determination via electron scattering: Heterogeneous Cu(001)–Pd surface alloy," *Phys. Rev. B*, vol. 76, no. 20, pp. 205414-1–205414-10, Nov. 2007.
12. J. B. Hannon, J. Sun, K. Pohl, and G. L. Kellogg, "Origins of nanoscale heterogeneity in ultrathin films," *Phys. Rev. Lett.*, vol. 96, no. 24, pp. 246103-1–246103-4, Jun. 2006.
13. S. Doğan, D. Johnstone, F. Yun, S. Sabuktagin, J. Leach, A. Baski, H. Morkoç, G. Li, and B. Ganguly, "The effect of hydrogen etching on 6H-SiC studied by temperature-dependent current–voltage and atomic force microscopy," *Appl. Phys. Lett.*, vol. 85, no. 9, pp. 1547–1549, Aug. 2004.
14. S. Soubatch, S. E. Saddow, S. P. Rao, W. Y. Lee, M. Konuma, and U. Starke, "Structure and morphology of 4H-SiC wafer surfaces after H₂-etching," *Mater. Sci. Forum*, vol. 483–485, pp. 761–764, 2005.
15. J. B. Hannon, R. M. Tromp, N. V. Medhekar, and V. B. Shenoy, "Spontaneous formation and growth of a new polytype on SiC(0001)," *Phys. Rev. Lett.*, vol. 103, no. 25, p. 256101, Dec. 2009.
16. J. E. Northrup and J. Neugebauer, "Theory of the adatom-induced reconstruction of the SiC(0001) $\sqrt{3} \times \sqrt{3}$ surface," *Phys. Rev. B*, vol. 52, no. 24, pp. R17001–R17004, Dec. 1995.
17. M. Sabisch, P. Krüger, and J. Pollmann, "Ab initio calculations of structural and electronic properties of 6H-SiC(0001) surfaces," *Phys. Rev. B*, vol. 55, no. 16, pp. 10 561–10 570, Apr. 1997.
18. A. Coati, M. Sauvage-Simkin, Y. Garreau, R. Pinchaux, T. Argunova, and K. Aid, "($\sqrt{3} \times \sqrt{3}$)R30° reconstruction of the 6H-SiC(0001) surface: A simple T₄ Si adatom structure solved by grazing-incidence X-ray diffraction," *Phys. Rev. B*, vol. 59, no. 19, pp. 12 224–12 227, May 1999.
19. T. Fujino, T. Fuse, J.-T. Ryu, K. Inudzuka, Y. Yamazaki, M. Katayama, and K. Oura, "Structural analysis of 6H-SiC(0001) $\sqrt{3} \times \sqrt{3}$ reconstructed surface," *Jpn. J. Appl. Phys.*, vol. 39, pp. 6410–6412, 2000.
20. Y. Han, T. Aoyama, A. Ichimiya, Y. Hisada, and S. Mukainakano, "Atomic models of ($\sqrt{3} \times \sqrt{3}$)R30° reconstruction on hexagonal 6H-SiC(0001) surface," *J. Vac. Sci. Technol. B*, vol. 19, no. 5, pp. 1972–1975, Sep. 2001.
21. M. C. Righi, C. A. Pignedoli, G. Borghi, R. Di Felice, C. M. Bertoni, and A. Catellani, "Surface-induced stacking transition at SiC(0001)," *Phys. Rev. B*, vol. 66, no. 4, pp. 045320-1–045320-7, Jul. 2002.
22. X. N. Xie, N. Yakolev, and K. P. Loh, "Distinguishing the H₃ and T₄ silicon adatom model on 6H-SiC(0001) $\sqrt{3} \times \sqrt{3}$ R30° reconstruction by dynamic rocking beam approach," *J. Chem. Phys.*, vol. 119, no. 3, pp. 1789–1793, Jul. 2003.
23. G. Zampieri, S. Lizzit, L. Petaccia, A. Goldoni, A. Baraldi, M. Bremholm, J. E. Gayone, S. V. Hoffmann, and P. Hofmann, "Photoelectron diffraction study of the 6H-SiC(0001) $\sqrt{3} \times \sqrt{3}$ R30° reconstruction," *Phys. Rev. B*, vol. 72, no. 16, pp. 165327-1–165327-9, Oct. 2005.
24. U. Starke, J. Schardt, J. Bernhardt, M. Franke, and K. Heinz, "Stacking transformation from hexagonal to cubic SiC induced by surface reconstruction: A seed for heterostructure growth," *Phys. Rev. Lett.*, vol. 82, no. 10, pp. 2107–2110, Mar. 1999.
25. M. A. Van Hove and S. Y. Tong, *Surface Crystallography by LEED*. Berlin, Germany: Springer-Verlag, 1979.
26. A. Barbieri and M. A. van Hove. [Online]. Available: <http://www.ap.cityu.edu.hk/personal-website/Van-Hove.htm>
27. J. B. Pendry, "Reliability factors for LEED calculations," *J. Phys. C*, vol. 13, no. 5, pp. 937–944, Feb. 1980.
28. M. A. Van Hove, W. H. Weinberg, and C. M. Chan, *Low-Energy Electron Diffraction*. New York: Springer-Verlag, 1986.
29. J. E. Demuth, P. M. Marcus, and D. W. Jepsen, "Analysis of low-energy-electron-diffraction intensity spectra for (001), (110), and (111) nickel," *Phys. Rev. B*, vol. 11, no. 4, pp. 1460–1474, Feb. 1975.
30. J. R. Noonan, H. L. Davis, and L. H. Jenkins, "LEED analysis of a Cu(110) surface," *J. Vac. Sci. Technol.*, vol. 15, no. 2, pp. 619–621, Mar. 1978.
31. H. L. Davis and J. R. Noonan, "Cu(100) multilayer relaxation," *J. Vac. Sci. Technol.*, vol. 20, no. 3, pp. 842–845, Mar. 1982.
32. Y. Goldberg, M. E. Levinshtein, and S. L. Romyantsev, *Properties of Advanced Semiconductor Materials GaN, AlN, SiC, BN, SiC, SiGe*. New York: Wiley, 2001.

Received January 19, 2011; accepted for publication April 5, 2011

Jiebing Sun Department of Physics and Material Science Program, University of New Hampshire, Durham, NH 03824 USA (jiebingsun.research@gmail.com).

James B. Hannon IBM Research Division, Thomas J. Watson Research Center, Yorktown Heights, NY 10598 USA (jbhannon@us.ibm.com).

Rudolf M. Tromp IBM Research Division, Thomas J. Watson Research Center, Yorktown Heights, NY 10598 USA (rtromp@us.ibm.com).

Karsten Pohl Department of Physics and Material Science Program, University of New Hampshire, Durham, NH 03824 USA (karsten.pohl@unh.edu).